arXiv:hep-ph/9604221v1 2 Apr 1996

Search of Stop, Sbottom, and Stau at an e^+e^- Linear Collider with $\sqrt{s} = 0.5 - 2$ TeV*

A. Bartl[1], H. Eberl[2], S. Kraml[2],

W. Majerotto[2], W. Porod[1], A. Sopczak[3][†]

(1) Institut für Theoretische Physik, Universität Wien, A-1090 Vienna, Austria

(2) Institut für Hochenergiephysik, Österreichische Akademie der Wissenschaften, A-1050 Vienna, Austria

(3) DESY-Zeuthen, D-15738, Zeuthen, Germany

Abstract

We discuss pair production and decays of stops, sbottoms, and staus in e^+e^- annihilation in the energy range $\sqrt{s} = 500$ GeV to 2 TeV. We present numerical predictions within the Minimal Supersymmetric Standard Model for cross sections and decay rates. We study the stop discovery potential for $\sqrt{s} = 500$ GeV and 10 fb^{-1} integrated luminosity with full statistics background simulation.

---

1   Introduction

In the experimental search for supersymmetry (SUSY) particular attention is paid to those particles which are expected to be relatively light. The scalar top quark, the SUSY partner of the top quark, may be the lightest squark, and may even be the lightest visible SUSY particle (LVSP) [1, 2]. The stop can be light for two reasons: (i) Due to the large top Yukawa terms in the renormalization group equations, the scalar mass parameters of the stop can be much smaller than the corresponding parameters of the first and second generation squarks [3, 4]. (ii) The off-diagonal elements of the mass mixing matrix of the stop can be large, and this leads to strong $\widetilde{t}_L - \widetilde{t}_R$ mixing. If the parameter $\tan\beta$ is large enough ($\tan\beta \gtrsim 10$) the scalar bottom quark [5] or the scalar tau lepton could also be relatively light and even be the LVSP. The existence of a relatively light stop would have many interesting phenomenological implications. A light stop would significantly influence the branching ratios of the decays $Z^0 \to b\bar{b}$, $t \to bW$, $b \to s\gamma$ and some other physical observables (see, e.g. [6]).

   In this contribution we shall present results for the production of stops, sbottoms, and staus in e^+e^- annihilation at energies between $\sqrt{s} = 500$ GeV and 2 TeV and details on signal selection and background rejection for stop production at $\sqrt{s} = 500$ GeV and $\mathcal{L} = 10$ fb^{-1}. The production cross sections and the decay rates, and thus the discovery reach of these sfermions show a distinct dependence on the L–R mixing angles. The most important decay modes of these sfermions are those into fermions and neutralinos or charginos.

   Our framework is the Minimal Supersymmetric Standard Model (MSSM) [7] which contains the Standard Model (SM) particles, sleptons, $\widetilde{\ell}^{\pm}$, $\widetilde{\nu}_\ell$, squarks, $\widetilde{q}$, gluinos $\widetilde{g}$, two pairs of charginos, $\widetilde{\chi}_i^{\pm}$, $i = 1, 2$, four neutralinos, $\widetilde{\chi}_i^0$, $i = 1, \ldots, 4$, and five Higgs particles, h^0, H^0, A^0, $H^{\pm}$ [8]. The phenomenology of stops, sbottoms, staus, and their decay products is determined by the following parameters: M and M', the (soft breaking) $SU(2)$ and $U(1)$ gaugino masses, μ, the higgsino mass parameter, $\tan\beta = v_2/v_1$ (where v_1 and v_2 are the vacuum expectation values of the neutral members of the two Higgs doublets), and $M_{\widetilde{L}}$, $M_{\widetilde{E}}$, $M_{\widetilde{Q}}$, $M_{\widetilde{U}}$, $M_{\widetilde{D}}$, A_τ, A_t, A_b, which are soft–breaking parameters entering the mass mixing matrices of the stau, stop, and sbottom systems. We assume the GUT relations $M'/M = \frac{5}{3}\tan^2\Theta_W \approx 0.5$, and $m_{\widetilde{g}}/M = \alpha_s/\alpha_2 \approx 3$, where $m_{\widetilde{g}}$ is the gluino mass. Furthermore, we assume that the $\widetilde{\chi}_1^0$ is the lightest SUSY particle (LSP).

   The lower model independent mass bound for stops obtained at LEP is 45 GeV [9, 10]. Stronger limits up to 55 GeV are reported from the data taking at LEP at 130–140 GeV [11]. The D0 experiment at the TEVATRON excludes the mass range 40 GeV $\lesssim M_{\widetilde{t}} \lesssim 100$ GeV for the stop, if the mass difference $M_{\widetilde{t}} - m_{\widetilde{\chi}_1^0} \gtrsim 30$ GeV [12].

   In Section 2 we shortly review the basic facts about L–R mixing of stops, sbottoms, and staus, and present our numerical results for the production cross sections for unpolarized beams as well as for polarized e^- beams. In Section 3 we describe the decays of stops, sbottoms, and staus and present numerical results for the important

branching ratios. We also list the signatures which are expected to be relevant at $\sqrt{s} = 500$ GeV. In Section 4 we describe an event generator for $\tilde{t}_1 \bar{\tilde{t}}_1$ production and decay. In Section 5 experimental sensitivities are determined based on Monte Carlo simulations. Section 6 contains a summery.

2 Cross Sections for Pair Production of Stops, Sbottoms, and Staus

The SUSY partners of the SM fermions with left and right helicity are the left and right sfermions. In the case of the stop, sbottom and stau the left and right states are in general mixed. In the $(\tilde{f}_L, \tilde{f}_R)$ basis the mass matrix is [1, 8]

$$M_{\tilde{f}}^2 = \begin{pmatrix} M_{\tilde{f}_L}^2 & a_f m_f \\ a_f m_f & M_{\tilde{f}_R}^2 \end{pmatrix} \tag{1}$$

with

$$M_{\tilde{f}_L}^2 = M_{\tilde{F}}^2 + m_Z^2 \cos 2\beta (T_f^3 - e_f \sin^2 \Theta_W) + m_f^2, \tag{2}$$

$$M_{\tilde{f}_R}^2 = M_{\tilde{F}'}^2 + e_f m_Z^2 \cos 2\beta \sin^2 \Theta_W + m_f^2, \tag{3}$$

$$m_t a_t \equiv m_t (A_t - \mu \cot \beta), \quad m_b a_b \equiv m_b (A_b - \mu \tan \beta), \quad m_\tau a_\tau \equiv m_\tau (A_\tau - \mu \tan \beta), \tag{4}$$

where e_f and T_f^3 are the charge and the third component of weak isospin of the sfermion $\tilde{f}$, $M_{\tilde{F}} = M_{\tilde{Q}}$ for $\tilde{f}_L = \tilde{t}_L, \tilde{b}_L$, $M_{\tilde{F}} = M_{\tilde{L}}$ for $\tilde{f}_L = \tilde{\tau}_L$, $M_{\tilde{F}'} = M_{\tilde{U}}, M_{\tilde{D}}, M_{\tilde{E}}$ for $\tilde{f}_R = \tilde{t}_R, \tilde{b}_R, \tilde{\tau}_R$, respectively, and m_f is the mass of the corresponding fermion. Evidently, there can be strong $\tilde{t}_L$-$\tilde{t}_R$ mixing due to the large top quark mass. Similarly, for sbottoms and staus L–R mixing is non-negligible if $\tan \beta \gtrsim 10$. The mass eigenvalues for the sfermion $\tilde{f} = \tilde{t}, \tilde{b}, \tilde{\tau}$ are

$$M_{\tilde{f}_{1,2}}^2 = \frac{1}{2} \left(M_{\tilde{f}_L}^2 + M_{\tilde{f}_R}^2 \mp \sqrt{(M_{\tilde{f}_L}^2 - M_{\tilde{f}_R}^2)^2 + 4m_f^2 a_f^2} \right) \tag{5}$$

where $\tilde{t}_1$, $\tilde{b}_1$ and $\tilde{\tau}_1$ denote the lighter eigenstates.

It is well known that the cross section for $e^+ e^- \to \tilde{t}_1 \bar{\tilde{t}}_1$ depends on the stop–mixing parameters. In particular the $Z^0 \tilde{t}_1 \bar{\tilde{t}}_1$ coupling vanishes for the mixing angle $\Theta_{\tilde{t}} = 0.98$ [13]. The cross sections for $e^+ e^- \to \tilde{b}_1 \bar{\tilde{b}}_1$ and $e^+ e^- \to \tilde{\tau}_1 \bar{\tilde{\tau}}_1$ also show a characteristic dependence on their mixing angles. The $Z^0 \tilde{b}_1 \bar{\tilde{b}}_1$ coupling vanishes at $\Theta_{\tilde{b}} = 1.17$, and the $Z^0 \tilde{\tau}_1 \bar{\tilde{\tau}}_1$ coupling vanishes at $\Theta_{\tilde{\tau}} = 0.82$. The interference between the γ and Z^0 exchange contributions leads to characteristic minima of the cross sections for $e^+ e^- \to \tilde{f}_1 \bar{\tilde{f}}_1$ which occur at specific values of the mixing angles $\theta_{\tilde{f}}$. They are given by

$$\cos^2 \Theta_{\tilde{f}}|_{min} = \frac{e_f}{T_f^3} \sin^2 \Theta_W [1 + (1 - s/m_Z^2) F(\sin^2 \Theta_W)] \,. \tag{6}$$

The function $F(\sin^2\Theta_W)$ depends on the polarization of the e^- beam and is given by $F(\sin^2\Theta_W) = \cos^2\Theta_W(L_e + R_e)/(L_e^2 + R_e^2) \approx -0.22$, $F(\sin^2\Theta_W) = \cos^2\Theta_W/L_e \approx -2.9$, and $F(\sin^2\Theta_W) = \cos^2\Theta_W/R_e \approx 3.3$, for unpolarized, left and right polarized e^- beams, respectively, where $L_e = -\frac{1}{2} + \sin^2\Theta_W$ and $R_e = \sin^2\Theta_W$. For polarized e^- beams the dependence on the mixing angles is much more pronounced than for unpolarized beams. The corresponding minima of the cross sections of $e^+e^- \rightarrow \tilde{f}_2\bar{\tilde{f}}_2$ occur at $1 - \cos^2\Theta_{\tilde{f}}|_{min}$.

In the calculations of the cross sections we have used the tree level formulae of [13, 15, 16]. We have also included SUSY QCD corrections taking the formulae of [17] (see also [13] and [18]) and corrections due to initial state radiation [19].

In Fig. 1a we show contour lines of the total cross section $e^+e^- \rightarrow \tilde{t}_1\bar{\tilde{t}}_1$ in the $M_{\tilde{t}_1} - \cos^2\Theta_{\tilde{t}}$ plane for $\sqrt{s} = 500$ GeV and unpolarized beams. For $M_{\tilde{t}_1} \simeq 100$ GeV this cross section can reach 220 fb. A substantial dependence on $\cos^2\Theta_{\tilde{t}}$ can be seen for $M_{\tilde{t}_1} \lesssim 150$ GeV. In Fig. 1b we show the $\cos^2\Theta_{\tilde{t}}$ dependence of the cross section $e^+e^- \rightarrow \tilde{t}_1\bar{\tilde{t}}_1$ for left and right polarized and unpolarized e^- beams for $\sqrt{s} = 500$ GeV and $M_{\tilde{t}_1} = 200$ GeV. The polarization asymmetry depends quite strongly on the mixing angle. Therefore, experiments with polarized e^- beams would be necessary for a precise determination of the mixing angle $\Theta_{\tilde{t}}$. The determination of the stop masses and mixing angle gives information on the basic SUSY parameters $M_{\tilde{Q}}$, $M_{\tilde{U}}$ and A_t. This is discussed in [14].

Similarly, Fig. 2 is a contour plot of the total cross section of $e^+e^- \rightarrow \tilde{t}_2\bar{\tilde{t}}_2$ in the $M_{\tilde{t}_2} - \cos^2\Theta_{\tilde{t}}$ plane at $\sqrt{s} = 2$ TeV, for left and right polarized e^- beams. Here we observe a strong dependence on the stop mixing angle. For $M_{\tilde{t}_2} \simeq 900$ GeV the cross section at this energy is about 1 fb.

In Fig. 3 we show the cross section for $e^+e^- \rightarrow \tilde{t}_1\bar{\tilde{t}}_2 + \bar{\tilde{t}}_1\tilde{t}_2$ at $\sqrt{s} = 1$ TeV as a function of $M_{\tilde{t}_1}$, for various values of $M_{\tilde{t}_2}$. Here we have fixed the mixing angle $\cos^2\Theta_{\tilde{t}} = 0.5$ where the cross section has its maximum. For other values of the mixing angle this cross section scales as $\sin^2\Theta_{\tilde{t}}\cos^2\Theta_{\tilde{t}}$. For $M_{\tilde{t}_1} \simeq 100$ GeV and $M_{\tilde{t}_2} \simeq 200$ GeV this cross section can reach 20 fb. Note that $e^+e^- \rightarrow \tilde{b}_1\bar{\tilde{b}}_2$ has the same cross section as $e^+e^- \rightarrow \tilde{t}_1\bar{\tilde{t}}_2$, if the masses and the mixing angles are the same (neglecting corrections due to gluino exchange). The cross section for $e^+e^- \rightarrow \tilde{\tau}_1\bar{\tilde{\tau}}_2$ is a factor of approximately 1/3 smaller because of the colour factor and the QCD radiative corrections which have to be included for squark production. Due to the factor $\sin^2\Theta_{\tilde{f}}\cos^2\Theta_{\tilde{f}}$, the cross section depends strongly on the mixing angle.

In Fig. 4a we show the contour plot of the total cross section of $e^+e^- \rightarrow \tilde{b}_1\bar{\tilde{b}}_1$ in the $M_{\tilde{b}_1} - \cos^2\Theta_{\tilde{b}}$ plane at $\sqrt{s} = 1$ TeV, for unpolarized beams. For $M_{\tilde{b}_1} \simeq 100$ GeV (450 GeV) this cross section can reach a value of about 50 fb (1 fb). For $M_{\tilde{b}_1} \lesssim 300$ GeV the cross section depends appreciably on $\cos^2\Theta_{\tilde{b}}$. For polarized e^- beams we have again a much stronger $\cos^2\Theta_{\tilde{b}}$ dependence of the cross sections, as shown in Fig. 4b
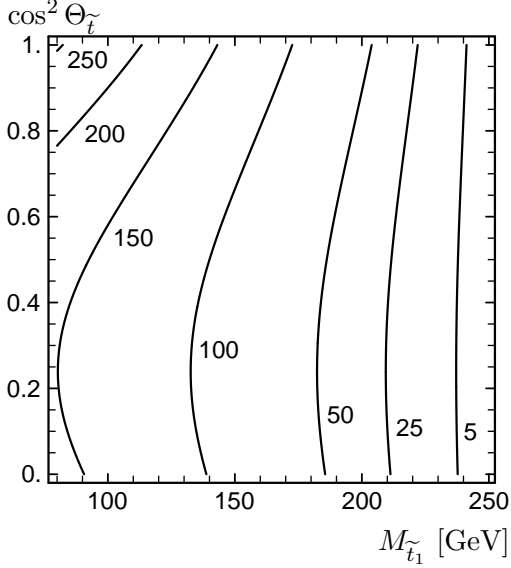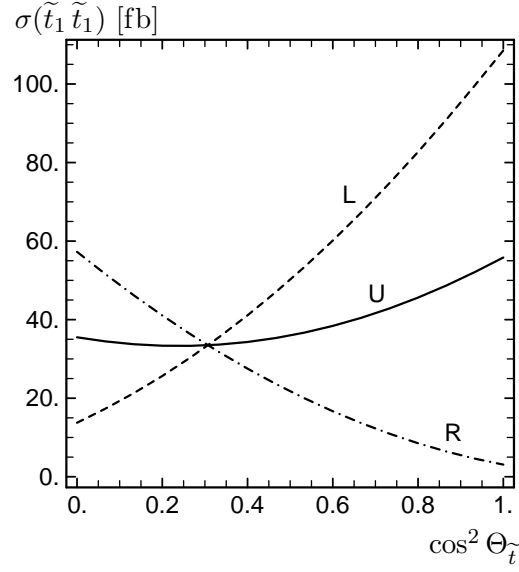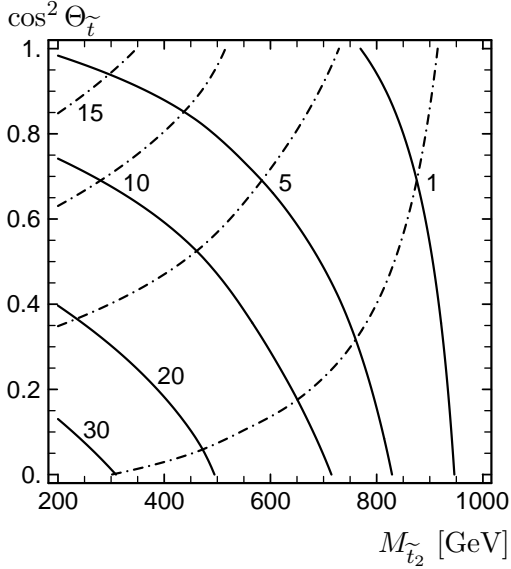
4

Fig. 1a: Contour lines for the total cross section of $e^+e^- \rightarrow \widetilde{t}_1 \bar{\widetilde{t}}_1$ in fb at $\sqrt{s} = 500$ GeV as a function of $\cos^2 \Theta_{\widetilde{t}}$ and $M_{\widetilde{t}_1}$.

Fig. 1b: Total cross section of $e^+e^- \rightarrow \widetilde{t}_1 \bar{\widetilde{t}}_1$ in fb at $\sqrt{s} = 500$ GeV as a function of $\cos^2 \Theta_{\widetilde{t}}$, for unpolarized (U) as well as left (L) and right (R) polarized e^- beams and $M_{\widetilde{t}_1} = 200$ GeV.

Fig. 2: Contour lines for the total cross section of $e^+e^- \rightarrow \widetilde{t}_2 \bar{\widetilde{t}}_2$ in fb at $\sqrt{s} = 2$ TeV as a function of $\cos^2 \Theta_{\widetilde{t}}$ and $M_{\widetilde{t}_2}$ for left (solid lines) and right (dashdotted lines) polarized e^- beams.
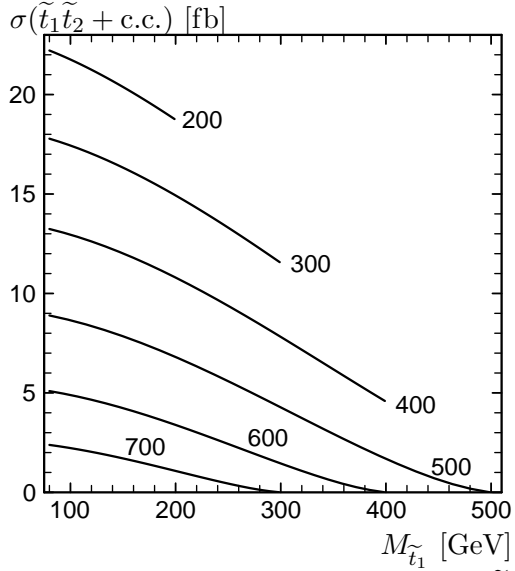

Fig. 3: Total cross section of $e^+e^- \rightarrow \widetilde{t}_1 \bar{\widetilde{t}}_2$ + c.c. in fb at $\sqrt{s} = 1$ TeV as a function of $M_{\widetilde{t}_1}$ for $\cos^2 \Theta_{\widetilde{t}} = 0.5$ and various masses of $\widetilde{t}_2$.
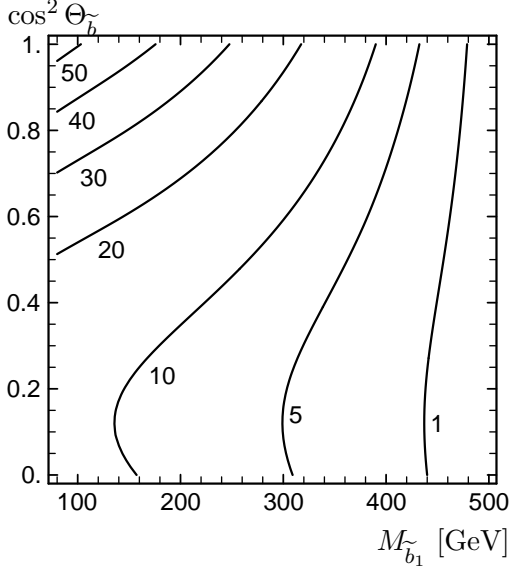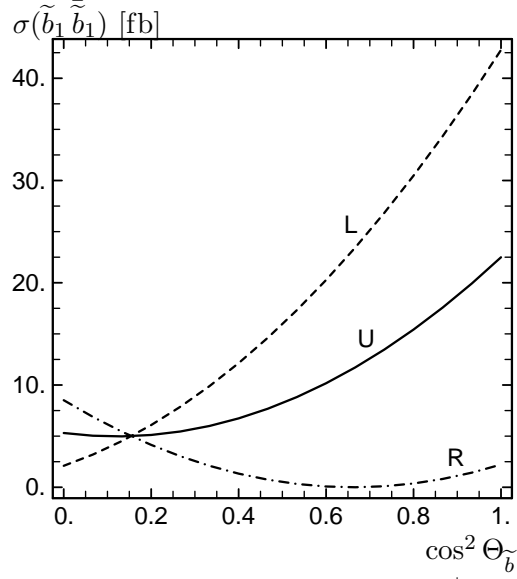
Fig. 4a: Contour lines for the total cross section of $e^+e^- \to \widetilde{b}_1 \bar{\widetilde{b}}_1$ in fb at $\sqrt{s} = 1$ TeV as a function of $\cos^2 \Theta_{\widetilde{b}}$ and $M_{\widetilde{b}_1}$.

Fig. 4b: Total cross section of $e^+e^- \to \widetilde{b}_1 \bar{\widetilde{b}}_1$ in fb at $\sqrt{s} = 1$ TeV as a function of $\cos^2 \Theta_{\widetilde{b}}$, for unpolarized (U), and left (L), and right (R) polarized e^- beams for $M_{\widetilde{b}_1} = 300$ GeV.
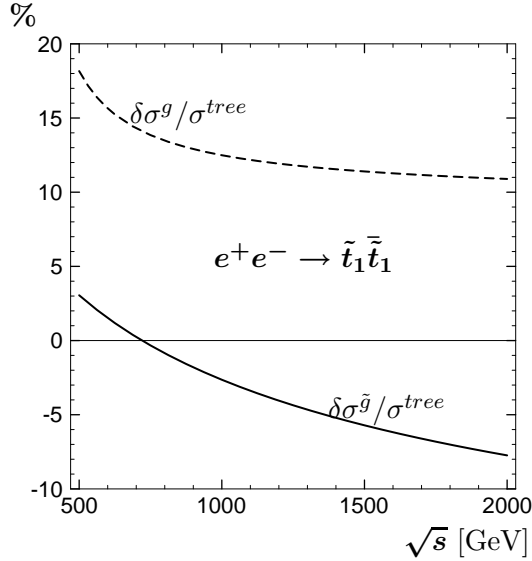

Fig. 5: SUSY–QCD corrections $\delta\sigma^g/\sigma^{tree}$ and $\delta\sigma^{\widetilde{g}}/\sigma^{tree}$ for $e^+e^- \to \widetilde{t}_1 \bar{\widetilde{t}}_1$ as a function of $\sqrt{s}$ for $\cos\Theta_{\widetilde{t}} = 0.7$, $M_{\widetilde{t}_1} = 150$ GeV, $M_{\widetilde{t}_2} = 300$ GeV and $M_{\widetilde{g}} = 300$ GeV.
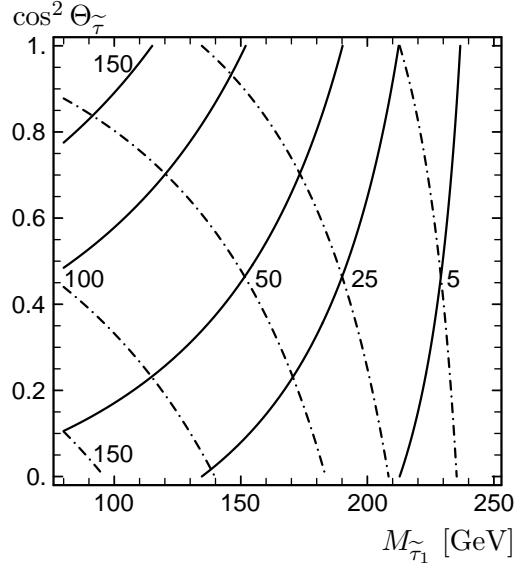

Fig. 6: Contour lines for the total cross section of $e^+e^- \to \widetilde{\tau}_1 \bar{\widetilde{\tau}}_1$ in fb at $\sqrt{s} = 500$ GeV as a function of $\cos^2 \Theta_{\widetilde{\tau}}$ and $M_{\widetilde{\tau}_1}$ for left (solid lines) and right (dashdotted lines) polarized e^- beams.

6

for $M_{\tilde{b}_1} = 300$ GeV and $\sqrt{s} = 1$ TeV.

The influence of the SUSY QCD corrections as a function of $\sqrt{s}$ is demonstrated in Fig. 5, where we have taken $\cos\Theta_{\tilde{t}} = 0.7$, $M_{\tilde{t}_1} = 150$ GeV, $M_{\tilde{t}_2} = 300$ GeV and $m_{\tilde{g}} = 300$ GeV. $\delta\sigma^g$ is the conventional QCD correction and $\delta\sigma^{\tilde{g}}$ is the correction due to gluino exchange. Note that at high energies $\delta\sigma^{\tilde{g}}$ has the opposite sign of $\delta\sigma^g$, and its absolute value is increasing with $\sqrt{s}$. For a more detailed discussion of SUSY QCD corrections see [17]. They increase the cross section values up to 40 %. The corrections due to initial state radiation turn out to be of the order of 10 %.

The cross sections for $e^+e^- \to \tilde{\tau}_1\bar{\tilde{\tau}}_1$ at $\sqrt{s} = 500$ GeV for left and right polarized e^- beams, as a function of $M_{\tilde{\tau}_1}$ and $\cos^2\Theta_{\tilde{\tau}}$ are shown in Fig. 6. For both beam polarizations these cross sections can reach values of approximately 150 fb, again exhibiting a strong dependence on the mixing angle.

3   Stop, Sbottom, and Stau Decays

The sfermions of the third generation can decay according to

$$\tilde{t}_i \quad \to \quad t\tilde{\chi}_k^0, \qquad b\tilde{\chi}_k^+ \tag{7}$$
$$\tilde{b}_i \quad \to \quad b\tilde{\chi}_k^0, \qquad t\tilde{\chi}_k^- \tag{8}$$
$$\tilde{\tau}_i \quad \to \quad \tau\tilde{\chi}_k^0, \qquad \nu_\tau\tilde{\chi}_k^+ \tag{9}$$

Due to the Yukawa terms and because of L–R mixing the decay patterns of stops, sbottoms, and staus will be different from those of the sfermions of the first two generations [20]. Stops and sbottoms may also decay into gluinos,

$$\tilde{t}_i \to t\tilde{g}, \qquad \tilde{b}_i \to b\tilde{g}, \tag{10}$$

and if these decays are kinematically allowed, then they are dominant. Otherwise, the decays (7), (8) are the most important ones. Moreover, in case of strong L–R mixing the splitting between the two mass eigenstates may be so large that the following additional decay modes are present [5]: $\tilde{t}_2 \to \tilde{t}_1 Z^0(h^0, H^0, A^0)$, $\tilde{b}_1 W^+(H^+)$, $\tilde{b}_2 \to \tilde{b}_1 Z^0(h^0, H^0, A^0)$, $\tilde{t}_1 W^-(H^-)$. The transitions $\tilde{t}_1 \to \tilde{b}_1 W^+(H^+)$ or $\tilde{b}_1 \to \tilde{t}_1 W^-(H^-)$ can occur if the mass difference is large enough.

If the $\tilde{t}_1$ is the LVSP and $m_{\tilde{\chi}_1^0} + m_b + m_W < M_{\tilde{t}_1} < m_{\tilde{\chi}_1^0} + m_t$, then the decay $\tilde{t}_1 \to b\,W^+\,\tilde{\chi}_1^0$ is important. If $M_{\tilde{t}_1} < m_{\tilde{\chi}_1^0} + m_b + m_W$ the higher–order decay $\tilde{t}_1 \to c\,\tilde{\chi}_1^0$ dominates [15]. In the parameter domain where $\tilde{t}_1 \to b\,W^+\,\tilde{\chi}_1^0$ is possible it is usually more important than $\tilde{t}_1 \to c\,\tilde{\chi}_1^0$. If $\tilde{b}_1$ or $\tilde{\tau}_1$ is the LVSP, then it decays according to $\tilde{b}_1 \to b\,\tilde{\chi}_1^0$ or $\tilde{\tau}_1 \to \tau\,\tilde{\chi}_1^0$. In the case that $M_{\tilde{\tau}_1} < M_{\tilde{t}_1}$ also $\tilde{t}_1 \to b\,\nu_\tau\,\tilde{\tau}_1$ may play a role.

In Fig. 7 a and b we show the parameter domains in the $M - \mu$ plane for the decays of $\tilde{t}_1$ and $\tilde{b}_1$, eqs. (7), (8), (10), taking $M_{\tilde{t}_1} = 400$ GeV, $\tan\beta = 2$, and $M_{\tilde{b}_1} = 400$ GeV, $\tan\beta = 30$, respectively. The parameter domains for the $\tilde{\tau}_1$ decays into neutralinos
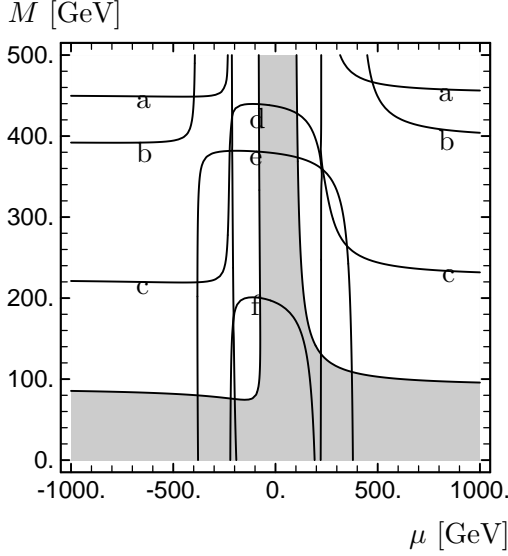
Fig. 7a: Kinematically allowed parameter domains in the (M, μ) plane for $M_{\tilde{t}_1} = 400$ GeV and $\tan\beta = 2$ for the decays: a) $\tilde{t}_1 \rightarrow t\tilde{\chi}_1^0$, b) $\tilde{t}_1 \rightarrow b\tilde{\chi}_1^+$, c) $\tilde{t}_1 \rightarrow t\tilde{\chi}_2^0$, d) $\tilde{t}_1 \rightarrow t\tilde{\chi}_3^0$, e) $\tilde{t}_1 \rightarrow b\tilde{\chi}_2^+$, f) $\tilde{t}_1 \rightarrow t\tilde{\chi}_4^0$. $\tilde{t}_1 \rightarrow c\tilde{\chi}_1^0$ and $\tilde{t}_1 \rightarrow bW^+\tilde{\chi}_1^0$ are allowed in the whole parameter range shown. The grey area is covered by LEP2 for $\sqrt{s} = 192$ GeV.
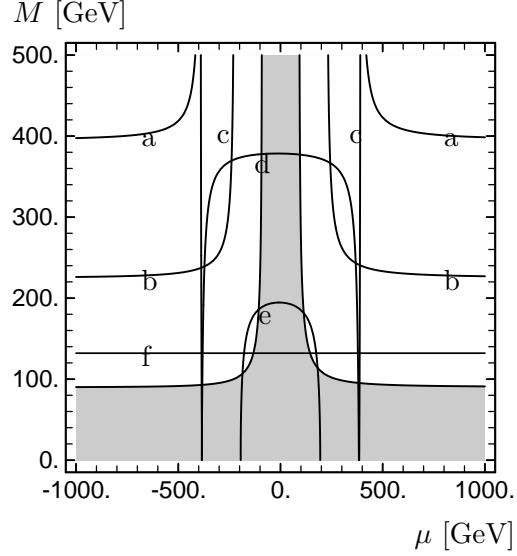
Fig. 7b: Kinematically allowed parameter domains in the (M, μ) plane for $M_{\tilde{b}_1} = 400$ GeV and $\tan\beta = 30$ for the decays: a) $\tilde{b}_1 \rightarrow b\tilde{\chi}_2^0$, b) $\tilde{b}_1 \rightarrow t\tilde{\chi}_1^-$, c) $\tilde{b}_1 \rightarrow b\tilde{\chi}_3^0$, d) $\tilde{b}_1 \rightarrow b\tilde{\chi}_4^0$, e) $\tilde{b}_1 \rightarrow t\tilde{\chi}_2^-$, f) $\tilde{b}_1 \rightarrow b\tilde{g}$. $\tilde{b}_1 \rightarrow b\tilde{\chi}_1^0$ is allowed in the whole parameter range shown. The grey area is covered by LEP2 for $\sqrt{s} = 192$ GeV.

are almost identical to those of the corresponding $\tilde{b}_1$ decays, if the masses of $\tilde{\tau}_1$ and $\tilde{b}_1$ are the same.

The branching ratios for the $\tilde{t}_1$ decays as a function of the mixing angle $\cos\Theta_{\tilde{t}}$ are shown in Fig. 8a for $M_{\tilde{t}_1} = 400$ GeV, $\tan\beta = 2$, and taking $M = 150$ GeV and $\mu = 500$ GeV. The decay into $b\tilde{\chi}_1^+$ dominates near $\cos\Theta_{\tilde{t}} = \pm 1$, $\tilde{t}_1 \approx \tilde{t}_L$, whereas the decay into $t\tilde{\chi}_1^0$ dominates near $\cos\Theta_{\tilde{t}} = 0$, $\tilde{t}_1 \approx \tilde{t}_R$. $\mathrm{BR}(\tilde{t}_1 \rightarrow b\tilde{\chi}_1^+)$ vanishes for $\cos\Theta_{\tilde{t}} \approx -0.3$ because gauge coupling and Yukawa coupling terms cancel each other. On the other hand, $\mathrm{BR}(\tilde{t}_1 \rightarrow t\tilde{\chi}_1^0)$ has a maximum for $\cos\Theta_{\tilde{t}} \approx -0.3$ because the two contributions add up. Similarly, Fig. 8b exhibits the branching ratios for the $\tilde{b}_1$ decays as a function of $\cos\Theta_{\tilde{b}}$ for $M_{\tilde{b}_1} = 400$ GeV, $\tan\beta = 30$, $M = 150$ GeV and $\mu = 500$ GeV. Here the branching ratio for the decay into $t\tilde{\chi}_1^-$ is smaller than that of $\tilde{t}_1 \rightarrow b\tilde{\chi}_1^+$, because it has less phase space. For $\tan\beta \gtrsim 10$ the branching ratios are almost symmetric under the simultaneous interchange $\mu \leftrightarrow -\mu$ and $\cos\Theta_{\tilde{t}} \leftrightarrow -\cos\Theta_{\tilde{t}}$. Note that in supergravity models [4], for large $\tan\beta$ and large $|\mu|$, $\cos\Theta_{\tilde{b}}$ has the same sign as μ, because otherwise the parameter A_b would be too large (see eq.(3)).

In Table 1 we list the most important signatures for $\tilde{t}_1$, $\tilde{b}_1$ and $\tilde{\tau}_1$ for $\sqrt{s} = 500$ GeV. If the decays $\tilde{t}_1 \rightarrow b\tilde{\chi}_1^+$ or $\tilde{\tau}_1 \rightarrow \nu_\tau\tilde{\chi}_1^-$ occur, the $\tilde{\chi}_1^\pm$ would be discovered first and

its properties would be known. This would help identify these events. The decay $\tilde{t}_1 \to b\,W^+\,\tilde{\chi}_1^0$ leads to the same final states as $\tilde{t}_1 \to b\,\tilde{\chi}_1^+$ (provided $\tilde{\chi}_1^+ \to H^+\tilde{\chi}_1^0$ is not allowed). From the decay $\tilde{\tau}_1 \to \tau\,\tilde{\chi}_1^0$ information about the neutralino parameters can be obtained by measuring the τ polarization, as discussed in [21].
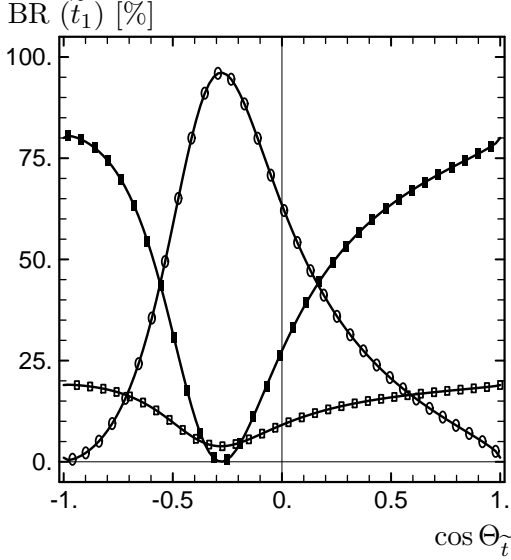

Fig. 8a: Branching ratios for the $\tilde{t}_1$ decays as a function of the mixing angle $\cos\Theta_{\tilde{t}}$ for $M_{\tilde{t}_1} = 400$ GeV, $\tan\beta = 2$, $M = 150$ GeV, and $\mu = 500$ GeV. The curves correspond to the following transitions: $\circ\ \tilde{t}_1 \to t\,\tilde{\chi}_1^0$, $\square\ \tilde{t}_1 \to t\,\tilde{\chi}_2^0$, $\blacksquare\ \tilde{t}_1 \to b\,\tilde{\chi}_1^+$.
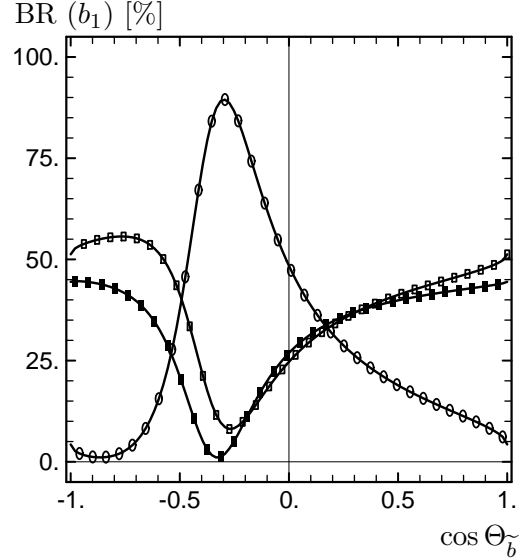
Fig. 8b: Branching ratios for the $\tilde{b}_1$ decays as a function of $\cos\Theta_{\tilde{b}}$ for $M_{\tilde{b}_1} = 400$ GeV, $\tan\beta = 30$, $M = 150$ GeV, and $\mu = 500$ GeV. The curves correspond to the following transitions: $\circ\ \tilde{b}_1 \to b\,\tilde{\chi}_1^0$, $\square\ \tilde{b}_1 \to b\,\tilde{\chi}_2^0$, $\blacksquare\ \tilde{b}_1 \to t\,\tilde{\chi}_1^-$.

	Signatures
$\tilde{t}_1 \to b\,\tilde{\chi}_1^+$	1 b-jet + 1 l^+ + $\not{p}_T$, 1 b-jet + 2 jets + $\not{p}_T$
$\tilde{t}_1 \to c\,\tilde{\chi}_1^0$	1 jet + $\not{p}_T$
$\tilde{b}_1 \to b\,\tilde{\chi}_1^0$	1 b-jet + $\not{p}_T$
$\tilde{b}_1 \to b\,\tilde{\chi}_2^0$	1 b-jet + l^+l^- + $\not{p}_T$, 1 b-jet + 2 jets + $\not{p}_T$
$\tilde{\tau}_1 \to \tau\,\tilde{\chi}_1^0$	τ + $\not{p}_T$
$\tilde{\tau}_1 \to \tau\,\tilde{\chi}_2^0$	τ + l^+l^- + $\not{p}_T$, τ + 2 jets + $\not{p}_T$
$\tilde{\tau}_1 \to \nu_\tau\,\tilde{\chi}_1^-$	l^- + $\not{p}_T$, 2 jets + $\not{p}_T$

Table 1: Expected signatures for $\tilde{t}_1$, $\tilde{b}_1$, and $\tilde{\tau}_1$ production for $\sqrt{s} = 500$ GeV. Due to pair production all combinations of the corresponding signatures may occur.

4 Stop Event Generation

In this section we describe the event generator for $e^+e^- \to \widetilde{t}_1\overline{\widetilde{t}}_1$ with the stop decay modes $\widetilde{t}_1 \to c\widetilde{\chi}_1^0$ and $\widetilde{t}_1 \to b\widetilde{\chi}_1^+$. The chargino decays via $\widetilde{\chi}_1^+ \to W^+\widetilde{\chi}_1^0$, where W^+ can be either virtual or real. The event generator is based on the calculation of the 4-momenta distributions of the stop and antistop decay products $\widetilde{\chi}_1^0 c$ $\widetilde{\chi}_1^0\overline{c}$ and $\widetilde{\chi}_1^+ b$ $\widetilde{\chi}_1^-\overline{b}$. The large effects of QCD corrections are included in the cross section calculation. Stop production and decay have been defined as new processes in the PYTHIA program package [22]. The event generation process includes the modelling of hadronic final states.

In the first step of the event generation, initial state photons are emitted using the program package REMT [22] which takes into account the expected stop cross section from zero to the nominal center-of-mass energy. Beamstrahlung photons are emitted using the beam parameters of the NLC 1992 design. The effective center-of-mass energy is calculated for the initial production of the 4-momenta of the final-state particles. These 4-momenta are then boosted to the lab-frame according to the momentum of the emitted photons. For the hadronization process of the $c\overline{c}$ in the $\widetilde{\chi}_1^0 c$ $\widetilde{\chi}_1^0\overline{c}$ and of the $b\overline{b}$ in the $\widetilde{\chi}_1^+ b$ $\widetilde{\chi}_1^-\overline{b}$ decay mode, a color string with invariant mass of the quark-antiquark-system is defined. The possible gluon emission and hadronization are performed using the Lund model of string fragmentation with the PYTHIA program package [22]. The Peterson *et al.* [23] fragmentation parameters for the c- and b-quarks are used: $\epsilon_c = 0.03$ and $\epsilon_b = 0.0035$. Finally, short-lived particles decay into their observable final state. Details of the event generator and of a stop analysis at LEP2 energies are given in [24].

5 Simulation and Selection

The investigated background reactions and their cross sections are shown in Fig. 11. They are simulated for $\mathcal{L} = 10$ fb^{-1}, and 1000 signal events are simulated in the $\widetilde{\chi}_1^0 c\widetilde{\chi}_1^0\overline{c}$ and $\widetilde{\chi}_1^+ b\widetilde{\chi}_1^-\overline{b}$ decay channels. The L3 detector at CERN including the upgrades for LEP2 served as an example for an e^+e^- 500 GeV detector. Details of the parametric detector simulation are given in [25]. An important feature is the overall hadronic energy resolution of about 7%.

In both channels, the $\widetilde{\chi}_1^0$'s escape the detector and cause large missing energy. In the case $\widetilde{\chi}_1^0 c\widetilde{\chi}_1^0\overline{c}$, the c-quarks form mostly two acoplanar jets. A mass combination of $M_{\widetilde{t}_1} = 180$ GeV and $m_{\widetilde{\chi}_1^0} = 100$ GeV is investigated in detail. For $\widetilde{\chi}_1^+ b\widetilde{\chi}_1^-\overline{b}$ on average the visible energy is larger. In this channel, the mass combination $M_{\widetilde{t}_1} = 180$ GeV, $m_{\widetilde{\chi}_1^+} = 150$ GeV, and $m_{\widetilde{\chi}_1^0} = 60$ GeV has been studied. Typically four jets are formed, two from the b-quarks, and two from the boosted W's.

In the first step of the event selection, unbalanced hadronic events are selected

using the following selection requirements:

$$25 < \text{hadronic clusters} < 110, \qquad 0.2 < E_{vis}/\sqrt{s} < 0.7,$$

$$E_\parallel^{\text{imb}}/E_{\text{vis}} < 0.5, \qquad \text{Thrust} < 0.95, \qquad |\cos\theta_{\text{Thrust}}| < 0.7 \ .$$
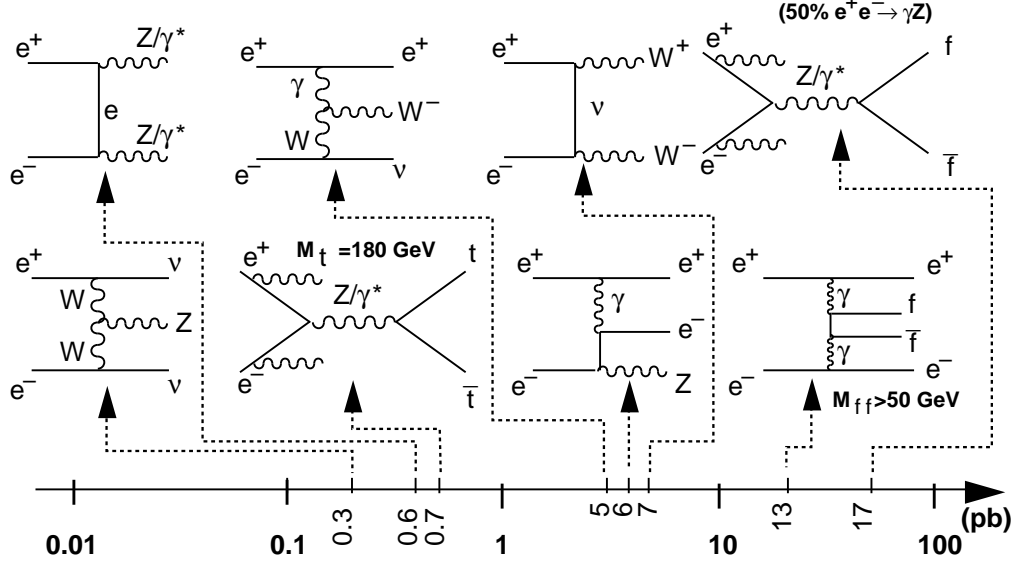

Figure 11: Background reactions and their cross sections for $\sqrt{s} = 500$ GeV.

Channel	$\tilde{\chi}_1^0 c \tilde{\chi}_1^0 \bar{c}$	$\tilde{\chi}_1^+ b \tilde{\chi}_1^- \bar{b}$	qq	WW	eWν	tt	ZZ	eeZ
Total (in 1000)	1	1	125	70	50	7	6	60
After preselection (in 1000)	0.4	0.7	1.7	2.2	3.2	1.3	0.2	0.3

Table 2: Expected events per 10 fb^{-1} at $\sqrt{s} = 500$ GeV, and number of events after the preselection as defined in the text.

A large part of the background of back-to-back events without missing energy is rejected. Table 2 shows the number of initially produced events per $\mathcal{L} = 10$ fb^{-1} at $\sqrt{s} = 500$ GeV, and the number of events which pass this preselection. The requirement of a large number of hadronic clusters removes e^+e^-, $\mu^+\mu^-$, and most $\tau^+\tau^-$ events. The minimum energy cut reduces most of the $\gamma\gamma$ events and ensures almost 100% trigger efficiency. The background from $\gamma\gamma$ events can, in addition, be strongly reduced by rejecting events where a scattered initial electron is detected at low angles. The upper energy cut reduces all standard background reactions. Beam gas events and events where much energy goes undetected along the beam axis are removed by rejection of events with very large parallel imbalance. The thrust cut removes remaining $\tau^+\tau^-$ events and reduces largely $q\bar{q}$ and $Z^0 Z^0$ background. The $\cos\theta_{\text{Thrust}}$

11

cut removes events where most probably much energy escaped undetected along the beam axis.

The final $\tilde{\chi}_1^0 c \tilde{\chi}_1^0 \bar{c}$ event selection is summarized in Table 3. The following cuts are applied:

- A hard upper energy cut reduces all standard background except $eW\nu$ (Fig. 12).
- Jets are clustered using the JADE algorithm. The y-cut value is optimized to obtain two jets for the signal.
- Semileptonic decays of the top quark can induce missing energy. These events are partly removed by requiring no isolated electron or muon.
- Events with large longitudinal energy imbalance are removed where probably much energy escaped undetected along the beam axis.
- The invariant mass of the two jets is required to be larger than 120 GeV to remove almost entirely $eW\nu$ events (Fig. 13).
- The acoplanarity angle is defined as the angle between the jets in the plane perpendicular to the beam axis. A maximum value of 2.9 rad is important to reduce the remaining background.

The result of this study is 4.3% detection efficiency and 9 background events. A detection confidence level of 3σ (99.73%) is expected for a cross section of 23 fb. Expected signal and background are shown in Fig. 16.

Channel	$\tilde{\chi}_1^0 c \tilde{\chi}_1^0 \bar{c}$	qq	WW	$eW\nu$	tt	ZZ	eeZ
Total (in 1000)	1	125	70	50	7	6	60
After Preselection	391	1652	2163	3185	1259	182	318
$E_{vis}/\sqrt{s} < 0.4$	332	**202**	**285**	3032	**70**	**4**	**98**
Njet = 2	293	172	182	2892	**17**	3	72
No isolated e or μ	218	152	**98**	2757	**5**	3	**9**
$E_{\parallel}^{imb}/E_{vis} < 0.3$	185	**101**	70	2049	5	2	4
Invariant mass of jets>120GeV	52	**25**	**12**	**7**	1	0	0
Acoplanarity < 2.9rad	43	**0**	**5**	**3**	1	0	0

Table 3: Final event selection cuts, expected signal efficiencies, and the number of expected background events. Bold face numbers indicate major background reductions.

The final $\tilde{\chi}_1^+ b \tilde{\chi}_1^- \bar{b}$ event selection is summarized in Table 4. Here the cuts are:
- A hard lower energy cut reduces most of the $eW\nu$ background.
- Topologies with back-to-back jets are reduced by an upper cut on the event thrust (Fig. 14).
- A lower cut on the number of hadronic clusters reduces efficiently low-multiplicity background final states (Fig. 15).
- Jets are clustered using the JADE algorithm. The y-cut value is optimized to obtain four jets for the signal.

- Events with an isolated electron or muon are rejected.
- An upper cut on the visible energy reduces $q\overline{q}$, W^+W^-, and $t\overline{t}$ background.
- Finally, the remaining $t\overline{t}$ background events are reduced by requiring less than 30% perpendicular energy imbalance.

Concerning the number of b-quarks per event, the decay $\tilde{\chi}_1^+ b \tilde{\chi}_1^- \overline{b} \rightarrow W^+ \tilde{\chi}_1^0 b W^- \tilde{\chi}_1^0 \overline{b}$ leads to the same final states as expected for $t\overline{t}$ background. Therefore, the tagging of b-quarks has not proved to be efficient to reduce this background.

The result of this study is 4.5% detection efficiency and 8 background events. A detection confidence level of 3σ (99.73%) is expected for a cross section of 19 fb. Expected signal and background are shown in Fig. 16.
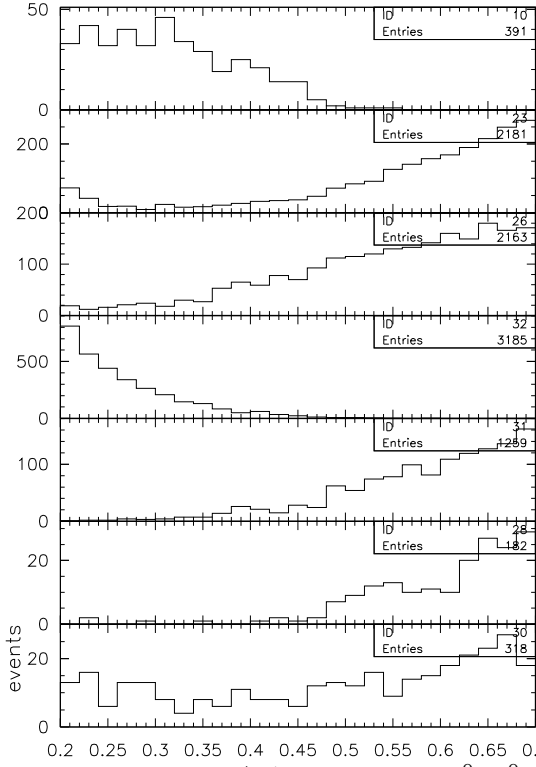
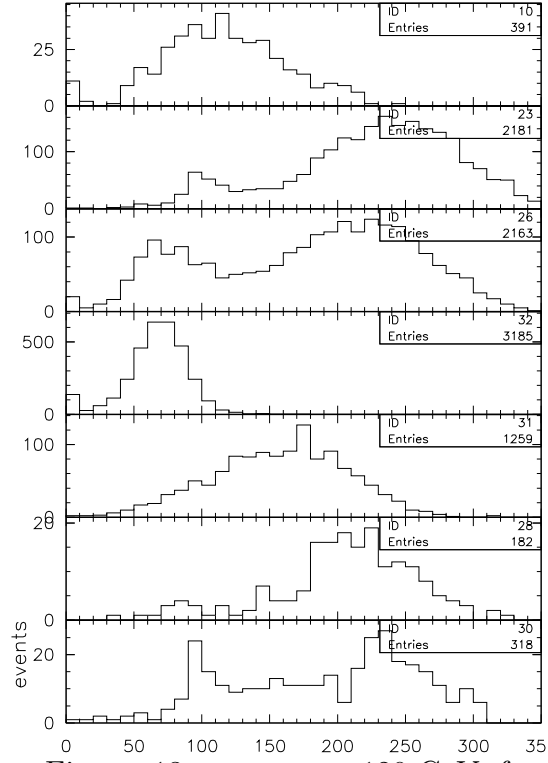Figure 12: $E_{vis}/\sqrt{s} < 0.4$ for $\tilde{\chi}_1^0 c \tilde{\chi}_1^0 \bar{c}$, qq, WW, eW$\nu$, tt, ZZ, eeZ.

Figure 13: $m_{\mathrm{inv}} > 120$ GeV for $\tilde{\chi}_1^0 c \tilde{\chi}_1^0 \bar{c}$, qq, WW, eW$\nu$, tt, ZZ, eeZ.
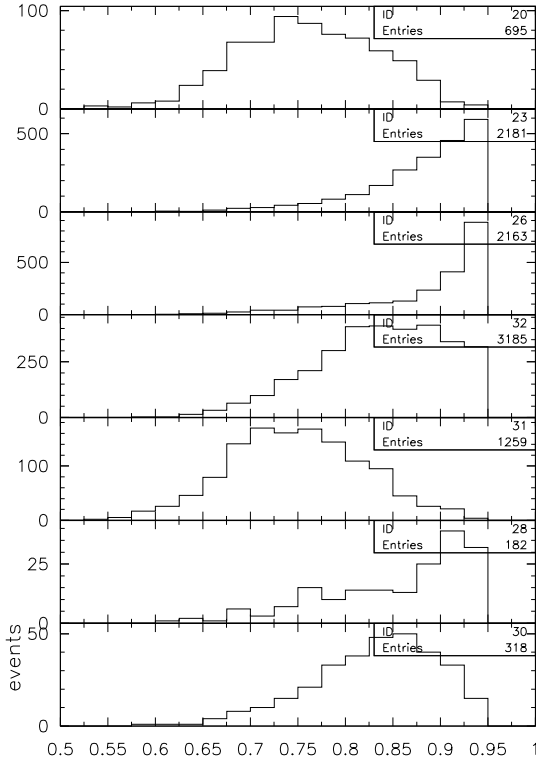

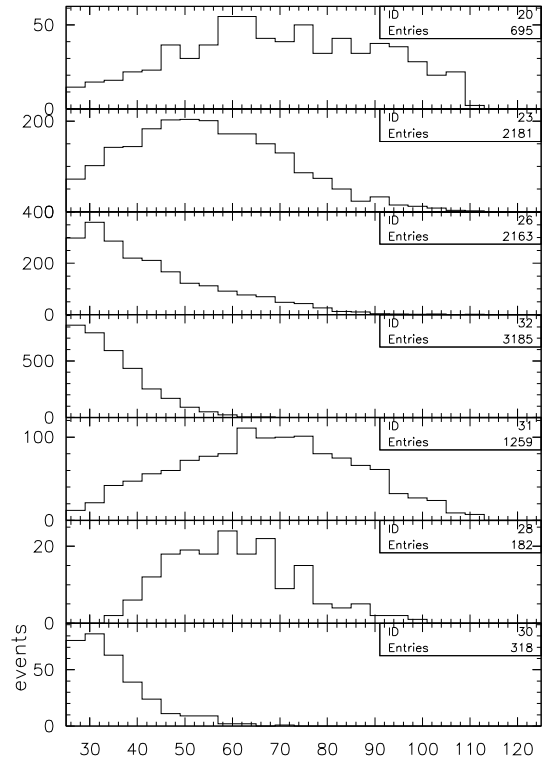Figure 14: Thrust < 0.85 for $\tilde{\chi}_1^+ b \tilde{\chi}_1^- \bar{b}$, qq, WW, eW$\nu$, tt, ZZ, eeZ.

Figure 15: Ncluster $\geq$ 60 for $\tilde{\chi}_1^+ b \tilde{\chi}_1^- \bar{b}$, qq, WW, eW$\nu$, tt, ZZ, eeZ.
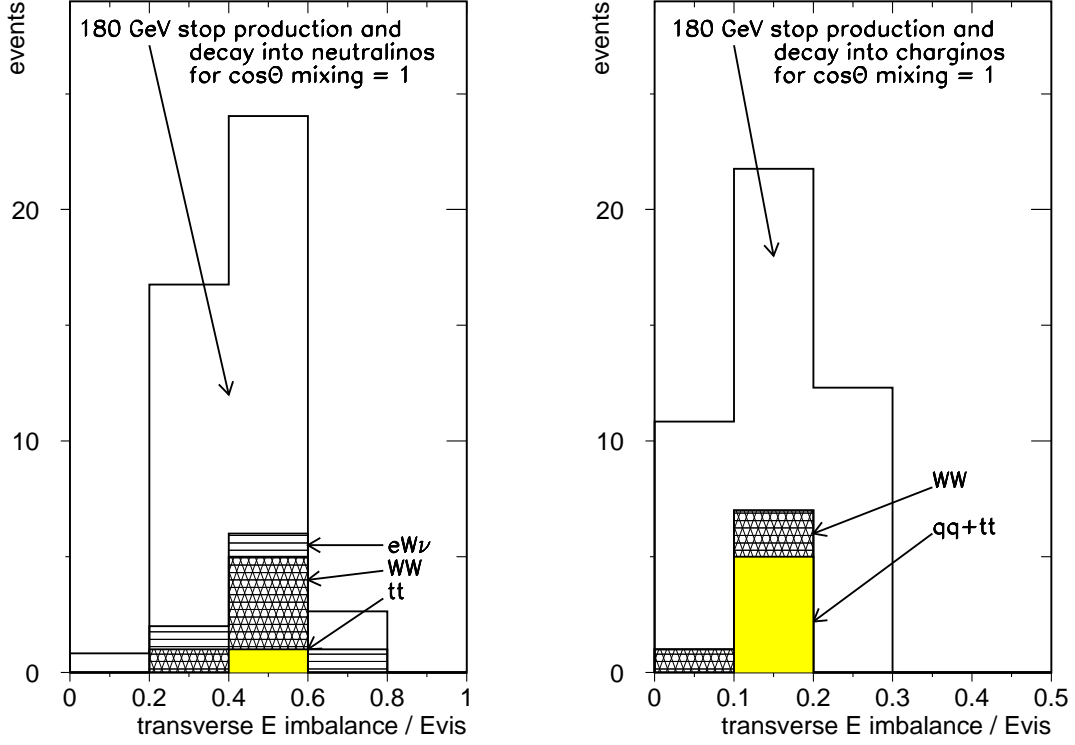
14

Figure 16: Left: Sensitivity for an $e^+e^- \to \tilde{t}_1 \bar{\tilde{t}}_1 \to \tilde{\chi}_1^0 c \tilde{\chi}_1^0 \bar{c}$ signal. Open histograms show the simulated signal, solid and hatched histograms show the remaining background after all selection cuts are applied. Right: Sensitivity for an $e^+e^- \to \tilde{t}_1 \bar{\tilde{t}}_1 \to \tilde{\chi}_1^+ b \tilde{\chi}_1^- \bar{b}$ signal.
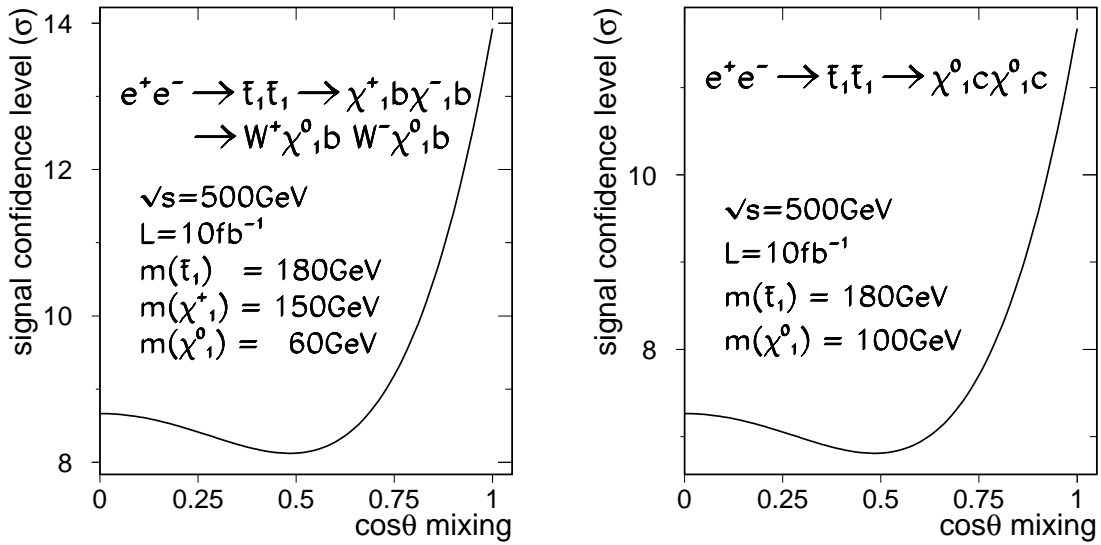

Figure 17: Detection confidence levels. Left: $\tilde{\chi}_1^+ b \tilde{\chi}_1^- \bar{b}$ channel. Right: $\tilde{\chi}_1^0 c \tilde{\chi}_1^0 \bar{c}$ channel.

Channel	$\widetilde{\chi}_1^+ b \widetilde{\chi}_1^- \bar{b}$	qq	WW	eWν	tt	ZZ	eeZ
Total (in 1000)	1	125	70	50	7	6	60
After Preselection	695	1652	2163	3185	1259	182	318
$E_{vis}/\sqrt{s} > 0.35$	610	1494	2011	**337**	1234	178	239
Thrust < 0.85	536	**326**	**420**	**24**	1141	**69**	137
Ncluster ≥ 60	399	195	**134**	**0**	769	41	**3**
Njet $= 4$	211	**53**	**72**	0	432	22	0
No isolated e or μ	99	41	49	0	**105**	16	0
$E_{vis}/\sqrt{s} < 0.55$	57	**3**	**8**	0	**23**	0	0
$E_\perp^{imb}/E_{vis} < 0.3$	45	1	3	0	**4**	0	0

Table 4: Final event selection cuts, expected signal efficiencies, and the number of expected background events. Bold face numbers indicate major background reductions.

At a future e^+e^- collider with $\sqrt{s} = 500$ GeV, a large discovery potential for scalar top quarks is already expected within one year of data-taking ($\mathcal{L} = 10$ fb^{-1}). Detector performances known from LEP detectors result in good background reduction. Full hermeticity of the detector is essential.

The confidence level for discovering a signal is shown in Fig. 17, where the confidence level is given in $\sigma = N_{\text{expected}}/\sqrt{N_{\text{background}}}$. The sensitivity is sufficient to discover a 200 GeV stop independently of the values of the mixing angle with 3σ in both $\tilde{\chi}_1^0 c$ and $\tilde{\chi}_1^+ b$ decay modes for the investigated neutralino and chargino mass combinations. A complete set of mass combinations remains to be studied. Beam polarization could be crucial for determining the stop mass after a discovery.

6 Summary

In this contribution we have discussed the production of stop, sbottom, and stau pairs in e^+e^- annihilation in the energy range $\sqrt{s} = 500$ GeV to 2 TeV. We have presented numerical predictions within the Minimal Supersymmetric Standard Model for the production cross sections and the decay rates and analyzed their SUSY parameter dependence. If $\tan\beta \gtrsim 10$, not only the t Yukawa terms, but also the b and τ Yukawa terms have important effects. The production cross sections as well as the decay rates of stops, sbottoms and staus depend in a characteristic way on the mixing angles.

A Monte Carlo study of $e^+e^- \to \tilde{t}_1 \bar{\tilde{t}}_1$ at $\sqrt{s} = 500$ GeV with the decays $\tilde{t}_1 \to c\,\tilde{\chi}_1^0$ and $\tilde{t}_1 \to b\,\tilde{\chi}_1^+$ has been performed for $M_{\tilde{t}_1} = 180$ GeV, $M_{\tilde{\chi}_1^0} = 100$ GeV, and $M_{\tilde{t}_1} = 180$ GeV, $M_{\tilde{\chi}_1^\pm} = 150$ GeV, $M_{\tilde{\chi}_1^0} = 60$ GeV, respectively. A suitable set of kinematical cuts has been applied to reduce the known background reactions. Detection confidence levels as a funtion of $\cos\Theta_{\tilde{t}}$ have been given. In summary, an e^+e^- collider is an ideal machine for detecting and studying scalar top and bottom quarks and scalar tau leptons.

Acknowledgements

References

[1] J. Ellis, S. Rudaz, Phys. Lett. B128 (1983) 248

[2] G. Altarelli, R. Rückl, Phys. Lett. B144 (1984) 126
I. Bigi, S. Rudaz, Phys. Lett. B153 (1985) 335

[3] W. de Boer, R. Ehret, D. I. Kazakov, Phys. Lett. B334 (1994) 220
W. de Boer et al., these proceedings

[4] See for a review e.g., M. Drees and S.P. Martin, Wisconsin preprint, MADPH-95-879

[5] A. Bartl, W. Majerotto, W. Porod, Z. Phys. C64 (1994) 499

[6] M. Fukugita, H. Murayama, M. Yamaguchi, T. Yanagida, Phys. Rev. Lett. 72 (1994) 3009
T. Kon, T. Nonaka, preprint ITP-SU-94/02, RUP-94-06
J. D. Wells, G. L. Kane, Phys. Rev. Lett. 76 (1996) 869
A. Brignole, F. Feruglio, F. Zwirner, CERN-TH/95-340

[7] H.E. Haber, G.L. Kane, Phys. Rep. 117 (1985) 75

[8] J. F. Gunion, H. E. Haber, Nucl. Phys. B272 (1986) 1

[9] J.-F. Grivaz, Rapporteur Talk, International Europhysics Conference on High Energy Physics, Brussels, 1995

[10] OPAL Collaboration, R. Akers et al., Phys. Lett. B337 (1994) 207
ALEPH Collaboration, Contribution #0416 to the International Europhysics Conference on High Energy Physics, Brussels, 1995

[11] ALEPH Collaboration, CERN-PPE/96-10, Jan. 1996
H. Nowak and A. Sopczak, L3 Note 1887, Jan. 1996
S. Asai and S. Komamiya, OPAL Physics Note PN-205, Feb. 1996

[12] D0 Collaboration, FERMILAB-Conf-95/393-E, Proc. of the 10th Topcial Workshop on "Proton–Antiproton Collider Physics", FNAL (1995)

[13] M. Drees, K. I. Hikasa, Phys. Lett. B252 (1990) 127

[14] A. Bartl, H. Eberl, W. Majerotto, W. Porod, Proc. of the US-Polish Workshop "Physics from Planck Scale to Electroweak Scale", Warshsaw 1994, p. 370, World Scientific (P. Nath, T. Taylor, S. Pokorski eds.)

[15] K. I. Hikasa, M. Kobayashi, Phys. Rev. D36 (1987) 724

[16] A. Bartl, H. Eberl, S. Kraml, W. Majerotto, W. Porod, preprint UWThPh-1996-18, HEPHY-PUB 642/96

[17] H. Eberl, A. Bartl, W. Majerotto, preprint UWThPh-1996-6, HEPHY-PUB 640/96

[18] W. Beenakker, R. Höpker, P. M. Zerwas, Phys. Lett. B349 (1995) 463

[19] See e.g. M. Peskin, 17th SLAC Summer Institute, SLAC-PUB-5210 (1990)

[20] A. Bartl, W. Majerotto, B. Mösslacher, N. Oshimo, S. Stippel, Phys. Rev. D43 (1991) 2214

[21] M. Nojiri, Phys. Rev. D51 (1995) 6281

[22] T. Sjöstrand, Comp. Phys. Comm. 82 (1994) 74

[23] C. Peterson *et al.*, Phys. Rev. D27 (1983) 105

[24] A. Sopczak, L3 note #1860 (1995), to be published in the LEP2 CERN Workshop report

[25] A. Sopczak, Proc. Workshop on physics and experiments with linear e^+e^- colliders, Waikoloa, Hawaii, USA, 26–30 April 1993 (World Scientific) p. 666; Z. Phys. C65 (1995) 449